Journal of Biomedical Optics

BiomedicalOptics.SPIEDigitalLibrary.org

Visualization of vasculature using a hand-held photoacoustic probe: phantom and *in vivo* validation

H. Maarten Heres
Mustafa Umit Arabul
Marcel C. M. Rutten
Frans N. Van de Vosse
Richard G. P. Lopata

SPIE.

H. Maarten Heres, Mustafa Umit Arabul, Marcel C. M. Rutten, Frans N. Van de Vosse, Richard G. P. Lopata, "Visualization of vasculature using a hand-held photoacoustic probe: phantom and *in vivo* validation," *J. Biomed. Opt.* **22**(4), 041013 (2017), doi: 10.1117/1.JBO.22.4.041013.

Visualization of vasculature using a hand-held photoacoustic probe: phantom and *in vivo* validation

H. Maarten Heres,* Mustafa Umit Arabul, Marcel C. M. Rutten, Frans N. Van de Vosse, and Richard G. P. Lopata
Eindhoven University of Technology, Cardiovascular Biomechanics Group, Department of Biomedical Engineering, The Netherlands

Abstract. Assessment of microvasculature and tissue perfusion can provide diagnostic information on local or systemic diseases. Photoacoustic (PA) imaging has strong clinical potential because of its sensitivity to hemoglobin. We used a hand-held PA probe with integrated diode lasers and examined its feasibility and validity in the detection of increasing blood volume and (sub) dermal vascularization. Blood volume detection was tested in custom-made perfusion phantoms. Results showed that an increase of blood volume in a physiological range of 1.3% to 5.4% could be detected. The results were validated with power Doppler sonography. Using a motorized scanning setup, areas of the skin were imaged at relatively short scanning times (<10 s/cm^2) with PA. Three-dimensional visualization of these structures was achieved by combining the consecutively acquired cross-sectional images. Images revealed the epidermis and submillimeter vasculature up to depth of 5 mm. The geometries of imaged vasculature were validated with segmentation of the vasculature in high-frequency ultrasound imaging. This study proves the feasibility of PA imaging in its current implementation for the detection of perfusion-related parameters in skin and subdermal tissue and underlines its potential as a diagnostic tool in vascular or dermal pathologies. [DOI: 10.1117/1.JBO.22.4.041013]

Keywords: photoacoustic imaging; vasculature; validation; phantom; probe.

Paper 160606SSRR received Aug. 31, 2016; accepted for publication Jan. 3, 2017; published online Jan. 24, 2017.

1 Introduction

The clinical potential of photoacoustic (PA) imaging has not escaped attention over recent years. The modality combines high optical contrast with high spatial resolution and has numerous possible *in vivo* applications in structural and functional imaging, ranging from the cellular substructure to organ scale.[1] The preferential absorption of light in the visible and near-infrared region by hemoglobin makes PA imaging sensitive in the detection and visualization of (micro) vasculature.[2–4] Assessment of microvasculature function has diagnostic potential for a wide range of systemic (vascular) diseases.[5] Visualization of superficial microvasculature and sensitive assessment of blood volume dynamics is hypothesized to be of added value in several pathologies with cutaneous involvement, such as systemic sclerosis and dermatomyositis.[6–8] Imaging of superficial tissue is an appealing application for PA because only a limited imaging depth is required.[2] Several groups have shown how PA imaging, in different implementations and combined with other modalities, can be used to assess (sub) dermal vascular geometry and functioning *in vivo*. However, validation of these PA results with conventional imaging techniques is not common.

High-resolution PA imaging of dermal structures and vascularization has been demonstrated with PA microscopy, with either focused acoustic detection or focused optical excitation. An acoustic-resolution PA microscopy (PAM) system with a broadband, 50-MHz focused ultrasound (US) transducer was presented by Maslov et al.[9] The system has a lateral and axial resolution of 45 and 15 μm, respectively, and is able to visualize the microvasculature and melanoma to a depth of 3 mm.[10] Multiwavelength measurements were used to estimate hemoglobin oxygen saturation levels for individual vessels. Favazza et al.[11] demonstrated functional volumetric imaging of cutaneous vasculature in the human hand palm, with a slightly modified version of this system, operating at wavelengths of 561 and 570 nm. With optical-resolution PAM, spatial resolutions of a few micrometers can be achieved, but only up to a depth of about 1 mm because of defocusing of the optical beam.[12] The restricted imaging depth limits the clinical application of this technique.[13]

An interesting alternative for piezoelectric detectors in high-resolution PA imaging was proposed by Zhang et al.[14] They used an interferometric optical US mapping system based on a Fabry–Perot polymer film. The system is capable of imaging vasculature with high sensitivity and spatial resolution (<100 μm) but also at depths of several millimeters.[15] Recently, Zabihian et al.[8] used this interferometric concept in combination with optical coherence tomography to visualize vascular abnormalities and skin lesions in relation to several human skin pathologies. The mechanical scanning of the image area with these microscopy setups results in scanning times in the order of minutes per cm^2.

Also on a more macroscopic scale, different PA configurations have been developed for superficial vasculature imaging. A spherical, probe-based PA detection configuration was proposed by Deán-Ben and Razansky,[16] who showed three-dimensional (3-D) vasculature imaging in real time at a frame rate of 10 Hz with an effective spatial resolution of 0.2 mm. They showed PA measurements of blood volume and oxygenation changes in the human finger after occlusion, also reported by Buehler et al.,[17] for a comparable, two-dimensional (2-D)

*Address all correspondence to: H. Maarten Heres, E-mail: h.m.heres@tue.nl

1083-3668/2017/$25.00

spherical array system. In both studies, no validation of the measured vasculature geometry or blood volume was provided.

Niederhauser et al.[18] showed combined US and PA imaging with a planar detection geometry. Laser pulses ($\lambda = 760$ nm) were delivered to the imaging site through a fiber, and PA signals were detected using a 7.5-MHz linear array US transducer. They performed real-time PA imaging of the skin and subdermal vasculature with a spatial resolution of about 0.3 mm at a frame rate of 7.5 Hz. Many other groups showed the combination of PA with US imaging in a probe-based, hand-held implementation, using an external laser source.[19]

For clinical applications, PA imaging would benefit from an affordable implementation that allows for mobile and quick image acquisition. Recently, Daoudi et al.[20] presented the FULLPHASE probe, which is a hand-held PA probe with integrated diode lasers that is capable of combined PA and US imaging and is controlled by a commercially available US scanner.

In this paper, we investigate the feasibility of this PA configuration for the assessment of changes in blood volume. A phantom study was performed in which microchannel phantoms that mimic biological tissue with increasing vascular density and allow for both PA and US imaging were designed. The results of PA imaging are validated with power Doppler US (PDUS), a widely clinically available US-based technique that has already set a track record in the assessment of perfusion-related parameters, such as moving blood volume.[21,22] Furthermore, subdermal vasculature geometries in the human hand palm and wrist are visualized in 3-D by combining multiple 2-D PA acquisitions. These results are validated with manually segmented vascular geometries from conventional B-mode US imaging

2 Materials and Methods

2.1 *Phantom Preparation*

Cylindrical phantoms were made out of polymethyl methacrylate (PMMA) tubes (length = 40 mm, inner$\varnothing$ = 14 mm), filled with gelatin (300 g Bloom, FormX, Amsterdam, the Netherlands). An acoustic window was realized on both sides of the tube to allow PA and PDUS measurements (Fig. 1).

A 10% mass/volume solution of gelatin was heated to 45°C for 10 min. Under continuous stirring, 3×10^{-3} volume/volume (v/v)% black Indian ink (Royal Talens, The Netherlands) and 14 v/v% Intralipid® fat emulsion (Fresenius Kabi, Bad Homburg, Germany) were added to the gelatin solution to tune the optical properties to physiological values of muscle tissue ($\mu_a = 0.25$ cm^{-1} and $\mu_s' = 7$ cm^{-1} at $\lambda = 800$ nm).[23,24] The optical absorption of the used ink batch was verified with a plate reader (SynergyHT, Biotek, Winooski). Finally, Orgasol (ELF Atochem, Paris, France) was added (1 percent by weight) for acoustic scattering.

The PMMA tubes were placed in teflon holders and filled with gelatin. Needles ($\varnothing = 180$ μm, Seirin J-Type, SEIRIN-America, Weymouth) were inserted into the gelatin to create microchannels upon removal, after solidification of the gelatin. The alignment and separation of the needles were ensured by placing them into a teflon disc with drilled grids. After 24 h of cooling at 4°C, the tubes were taken out of the holders and the needles were removed from the gelatin. Four different phantoms were made with an increasing amount of channels, resulting in a total perfused cross-sectional area of 1.3%, 2.7%, 4.0%, and 5.4% respectively, which is in the physiological range of human skeletal muscle.[25,26]

2.2 *Probes*

PA imaging was performed using the second generation FULLPHASE prototype PA probe, controlled by a MyLab One scanner (ESAOTE Europe, Maastricht, The Netherlands). The integrated diode laser system (QUANTEL, France, OSRAM, Germany), consisting of a stack of highly efficient diode arrays in the probe, operates at $\lambda = 805$ nm with 1-mJ pulses. A customized laser driver (BRIGHTLOOP, France) allows a pulse width of 130 ns at half maximum and a maximum pulse repetition rate of 10 kHz. Using a combination of cylindrical lenses and diffractive optical elements (SILIOS, France), the beam is collimated and homogenized in the axis perpendicular to the diode arrays and reshaped into a rectangular form. The laser beam exits the probe through a small glass window. A linear array transducer (SL3323, $f_c = 7.5$ MHz, ESAOTE Europe, The Netherlands), next to the glass window (Fig. 2), constitutes the US transducer of the probe. The spatial resolution of the system is 0.28 mm axially and around 0.5 mm laterally, depending on the imaging depth. Further operation and specification details of the FULLPHASE probe can be found in the paper by Daoudi et al.[20]

PDUS imaging was performed using an LA523 probe in combination with a MyLab 70 scanner (ESAOTE Europe,

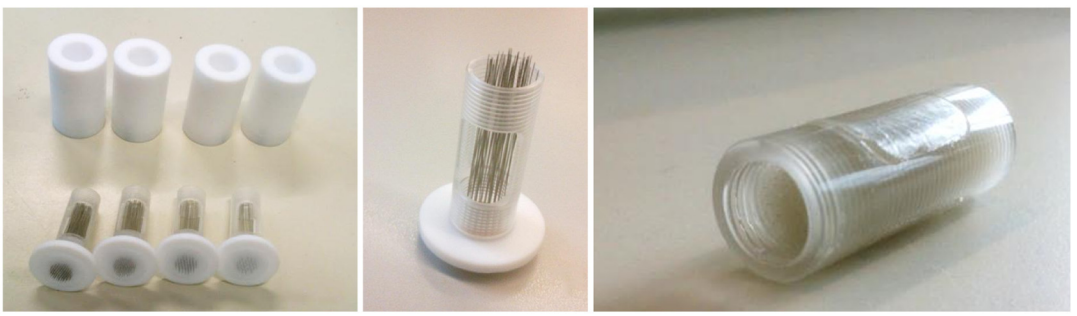

(a) (b) (c)

Fig. 1 Perfusion phantoms: (a) the cylindrical perfusion phantom molds, consisting of a cylindrical PMMA tube with a cut-away to enable acoustic measurements. (b) Needles are used to create channels in the gelatin. The mold is placed within a teflon holder and filled with gelatin.(c) After solidifying, the tube is taken out of the teflon holder and the needles are removed. On the inner wall of the tubes, a screw thread was tapped to prevent leakage and sliding of the gelatin during perfusion.

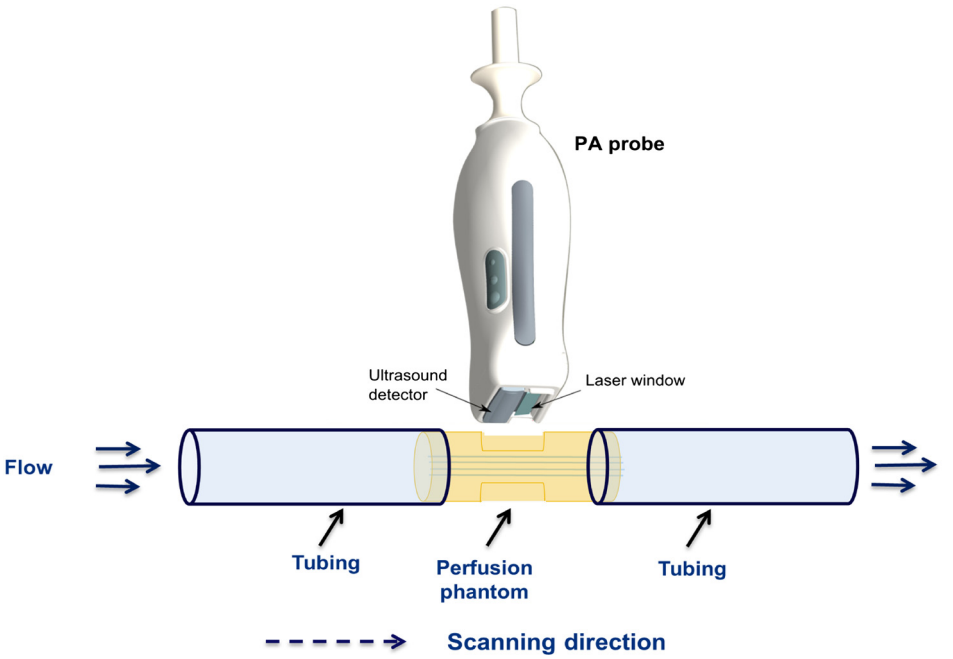

Fig. 2 Schematic of the imaging setup used in the phantom study. The image shows the PA probe, placed orthogonally above the phantom to obtain cross-sectional images.

Maastricht, The Netherlands). The element length (5 mm), pitch (0.245 mm), and center frequency (7.5 MHz) of this probe are similar to the US part of the FULLPHASE probe. For US measurements on vasculature, a high-frequency linear array probe was used (LA435, $f_c = 12$ MHz, pitch $= 0.2$ mm, ESAOTE Europe, The Netherlands) combined with the MyLab 70 scanner.

2.3 *Imaging Setup for Phantom Measurements*

The phantoms were connected to a syringe pump (STC-521, Terumo Europe, Leuven, Belgium) using silicone tubing and perfused with an ink solution (Fig. 2). The optical absorption of the ink solution (0.013% v/v) resembled that of diluted blood[27] at 805 nm (hematocrit $= 5\%$, $\mu_a = 1.0$ cm^{-1}). The pump flow rate was adjusted to establish an average flow velocity of 20 mm/s in all phantoms. A customized probe holder was used to place the PA and PDUS probe orthogonally above the phantoms. PA and PDUS imaging were performed during perfusion while the tubing, phantom, and probe tips were submerged in water at room temperature. Additionally, a motorized translation stage (M-403.2DG, Physik Instrumente, Germany) was used to move the PA probe horizontally over the phantom at a constant velocity during scanning, to allow for 3-D PA visualization, using the consecutive cross-sectional images at different locations to reconstruct a volume data set.

2.4 *Scanning Protocol for Phantom Measurements*

Cross-sectional images of each phantom at the center of the acoustic window were acquired, first with PDUS and then with PA. The distance between the US detector surface and the phantom surface was kept at 5 mm. In PDUS, the US frequency was set to 6.3 MHz and the pulse repetition frequency of the PDUS mode to 1.5 kHz, with the lowest possible wall filter setting. Data were acquired for 10 s at a frame rate of 33 Hz. In PA imaging, 100 frames were acquired at a frame rate of 40 Hz. Additionally, a PA scan was made over the whole length of the acoustic window (20 mm) using the motorized stage, at a constant velocity of 1.2 mm/s and a frame rate of 40 Hz.

2.5 *Data Processing and Analysis*

2.5.1 *Photoacoustic data*

Raw radio frequency (RF) data, stored at a sample frequency of 50 MHz, were reconstructed offline using MATLAB® (MATLAB® 2014b, MathWorks, Natick, Massachusetts). Multiple filtering steps were performed, i.e., DC blocking, moving average filtering ($N = 19$;), and bandpass filtering (0.8 to 5.5 MHz). The filter cutoff frequencies are based on a spectral analysis of the raw PA signal from superficial tissue and vasculature, obtained with this system, which typically showed strong signal contribution around 3.5 MHz. Next, the beam-formed RF data were reconstructed with the delay-and-sum method. To improve image quality, the individual frames in the beam-formed data were deconvolved with the Richardson–Lucy algorithm using the system's point spread function (PSF), measured on a cylindrical black object ($d = 100$ μm) at a depth of 10 mm. Forty consecutive frames were averaged, and the intensity was thresholded at −23 dB. This threshold is based on the SNR of the signal from the channel closest to the probe (in the upper part of the image), compared to the mean intensity value of the noise in the lower part of the image, where no channel signal is visible. An overview of the signal processing sequence is given in Fig. 3. In the resulting image, the visible cross-sectional area of the phantom was considered as the region of interest (ROI). The perfused cross-sectional area was calculated by dividing the amount of pixels in the ROI with an intensity level above the threshold by the total number of pixels in the masked area. Because of the limited penetration depth of the PA imaging (<8 mm), only the upper half of the phantoms was taken into account. A visualization of the reconstructed 3-D volume based on the PA scanning was realized using

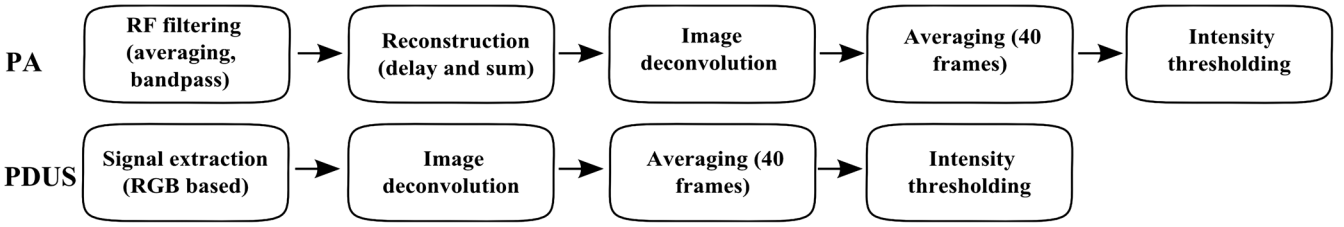

Fig. 3 Block diagram of the signal processing, for both PA and PDUS.

MATLAB® after stacking all acquired 2-D frames and thresholding the data at noise level.

2.5.2 *Power Doppler Ultrasound data*

Data sets of every measurement were exported as DICOM files and processed offline using MATLAB®. PDUS signals in the frames were extracted using the RGB values to discriminate them from B-mode gray values. The PDUS images were deconvolved using the signal of a single channel in the phantoms, which was considered as the PSF of PDUS imaging. The resulting values of 40 frames were averaged, as in PA, and the total phantom area was regarded as ROI. An intensity threshold of −30 dB was applied, to sufficiently reduce the blurring effect of averaging on the channel signal area. The amount of pixels within the ROI, with an intensity value above this threshold, was divided by the total number of pixels in the ROI, as a measure of perfused cross-sectional area.

2.6 *Scanning Setup and Protocol for In Vivo Photoacoustic Measurements*

To test the feasibility of visualizing skin and superficial blood vessel geometries using the FULLPHASE PA probe, a small area on the ball of the hand of a volunteer was imaged. Also, in four different volunteers, the skin on the inside of the wrist was imaged. The volunteer study was approved by the research ethics committee of the Radboud University Nijmegen Medical Centre (Nijmegen, The Netherlands), and requirements for informed consent were waived.

During scanning, the forearm of the volunteer and the tip of the probe were submerged in a water tank. To avoid vasoconstriction, the water was kept at a temperature of approximately 30°C. The probe was mounted in a custom-made probe holder and attached to the aforementioned translation stage [Fig. 4(a)]. After positioning the probe at a distance of 5 mm from the skin, areas of approximately 25 × 15 mm (image width) were imaged at a frame rate of 40 Hz, while again moving the probe at a constant velocity of 1.2 mm/s using the translation stage. The scanning method including a water tank and a translation stage [Fig. 4(b)] is related to the one described in the work by Fronheiser et al.[28] The scan area at the wrist was demarcated by water resistant band-aids, provided with ink lining [Fig. 4(c)]. This functioned as a marker in both PA and US imaging.

2.7 *Visualization of In Vivo Photoacoustic Measurements*

Data were filtered and reconstructed offline as described in the phantom study. The 2-D frames were stacked and intensities were thresholded at noise level (−23 dB) before 3-D renderings were reconstructed for visualization. For visualization purposes, the epidermis and underlying blood vessels were represented with a different color. Segmentation in each 2-D frame was performed automatically using the pronounced curved signal of the epidermis in the images.

2.8 *Validation of In Vivo Photoacoustic Measurements with Ultrasound*

To validate the PA blood vessel visualization in the wrist, the vessel geometry of the same area was also obtained with high-resolution US. In the same way as with PA, cross-sectional B-mode images were acquired at a frame rate of 40 Hz while moving the US probe over the skin. After transferring the DICOM data to an external PC, the skin contour and individual

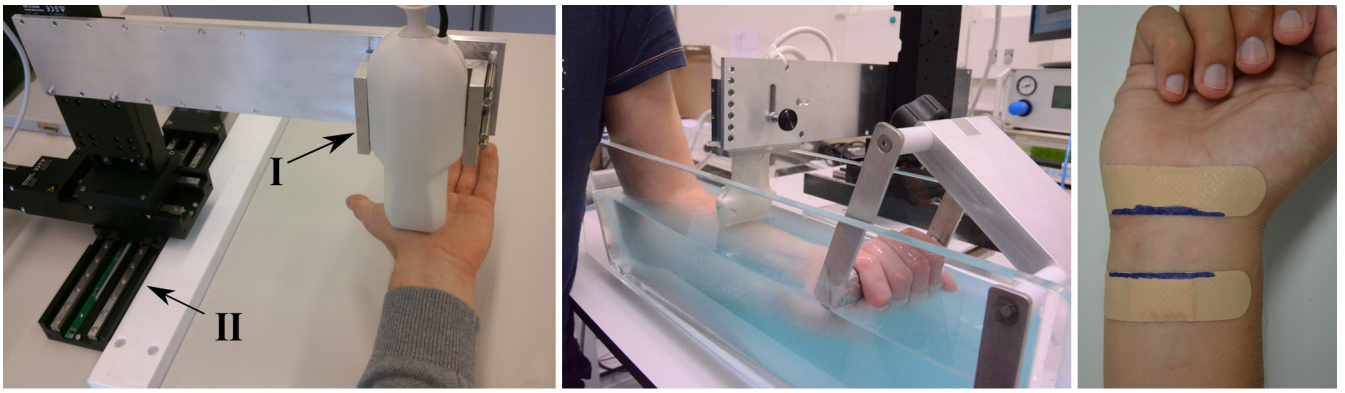

(a) (b) (c)

Fig. 4 PA setup for skin imaging. (a) The PA probe is mounted into a customized probe holder (I) and attached to the translation stage (II). (b) The water tank for *in vivo* scanning, showing the fixed handgrip for support. (c) The skin areas at the wrist are demarcated with band-aid and ink.

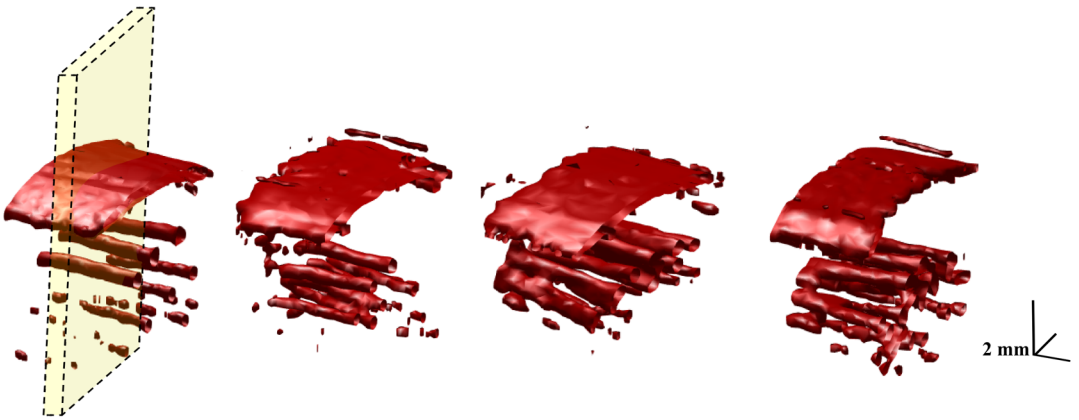

Fig. 5 3-D visualization of the PA scans of the phantoms. The four different phantoms are shown, with increasing perfused area from left to right. The yellow plane indicates the location of the cross-sectional images on which the analysis is performed.

vessels were manually segmented in selected frames, using MATLAB® software. By interpolating the manual segmentations over the whole data set, the contours of the vessels were reconstructed and visualized. The 3-D vascular geometries obtained in both PA and US were compared.

3 Results

3.1 *Phantom Measurements*

Figure 5 shows the 3-D rendered PA images of the four different phantoms. The signal originating from the upper edge of the phantom is clearly visible on top of the signals from the channels. Due to a limited depth of light penetration, only part of the channels is visible. The increase in the amount of channels can be appreciated from these images.

Figure 6 shows raw and processed PA and PDUS cross-sectional images of the four phantoms. In the raw images, the PDUS signal is represented by the red values. In the most perfused phantom (5.4%), the PDUS signal of several channels seems to overlap due to the limited resolution, creating an overshoot of signal. In PDUS, the whole phantom is clearly visible, showing the difference in imaging depth between PDUS and PA.

The measured amount of signal in each phantom is shown in Fig. 7, for both PA and PDUS. In PA, the relative amount of pixels that exceeded the intensity threshold seems to be proportional to the real perfused area in the phantoms. The results are validated with PDUS, where the same correlation is found. However, the visual overshoot of PDUS signal that was encountered in the cross-sectional images of the most perfused phantom is also found in the quantitative analysis.

3.2 *In Vivo Measurements*

An example of PA scans in the human hand is shown in Fig. 8. A typical cross-sectional image of these areas reveals a relatively strong, curved signal from melanin in the epidermis on top of signals from (sub) millimeter size blood vessels underneath. Another, low intensity, curved signal at the location of the deep vascular plexus is observed approximately 1 to 1.5 mm below the epidermis. The achieved imaging depth is around 5 mm. 3-D visualization shows the geometry of the vessels while segmentation offers the possibility of discriminating between epidermis and blood vessels. Total acquisition time for these areas of 3 cm^2 was 17 s.

Figure 9 shows the validation of *in vivo* PA vasculature imaging with high-frequency US imaging in four volunteers. The image width of US was 37 and 15 mm in PA. In the third volunteer, two PA scans on adjacent skin areas were combined. In the second volunteer, only one half of the scanned area could be used because of technical issues. In the acquired 2-D US images, the skin layer contour and the (sub) millimeter vasculature in the hypodermis could easily be observed up to a depth of 1 cm. In the 3-D renderings, white striped areas indicate the marking band-aid that was clearly visible in both modalities. The visualization of skin and vasculature shows the resemblance of the imaged vasculature geometries in both PA and US in terms of number of vessels and vessel size. The images also show that a higher resolution is obtained with US in this setup.

4 Discussion

In this study, we demonstrated the feasibility of PA measurements on perfusion-related parameters, blood volume and vascularization, using a hand-held PA probe with integrated diode lasers. Using conventional US imaging, we validated the results obtained with this PA implementation.

In a phantom study, we showed that an increase of blood volume in the physiological range of 1.3% to 5.4% is detectable with PA imaging. The relative amount of signal was proportional to the amount of perfused area in the phantom. This result was validated with PDUS, which showed the same proportional signal increase. A small overshoot of signal was measured with PDUS in the phantom with a 5.4% perfused area. This is due to the limited spatial resolution in PDUS, which leads to overlapping signals of neighboring channels. The results suggest that PA imaging, in its current configuration, can be used to visualize submillimeter vasculature and changes in blood volume in the physiological range.

For analysis, the acquired signals in both modalities were intensity thresholded based on image SNR (in PA) or based on empirical findings (in PDUS). This is sufficient for the assessment of sensitivity, as in this study, on the detection of an increasing blood volume. For comparison of modalities in true quantitative measurements, standardization of thresholding will be required.

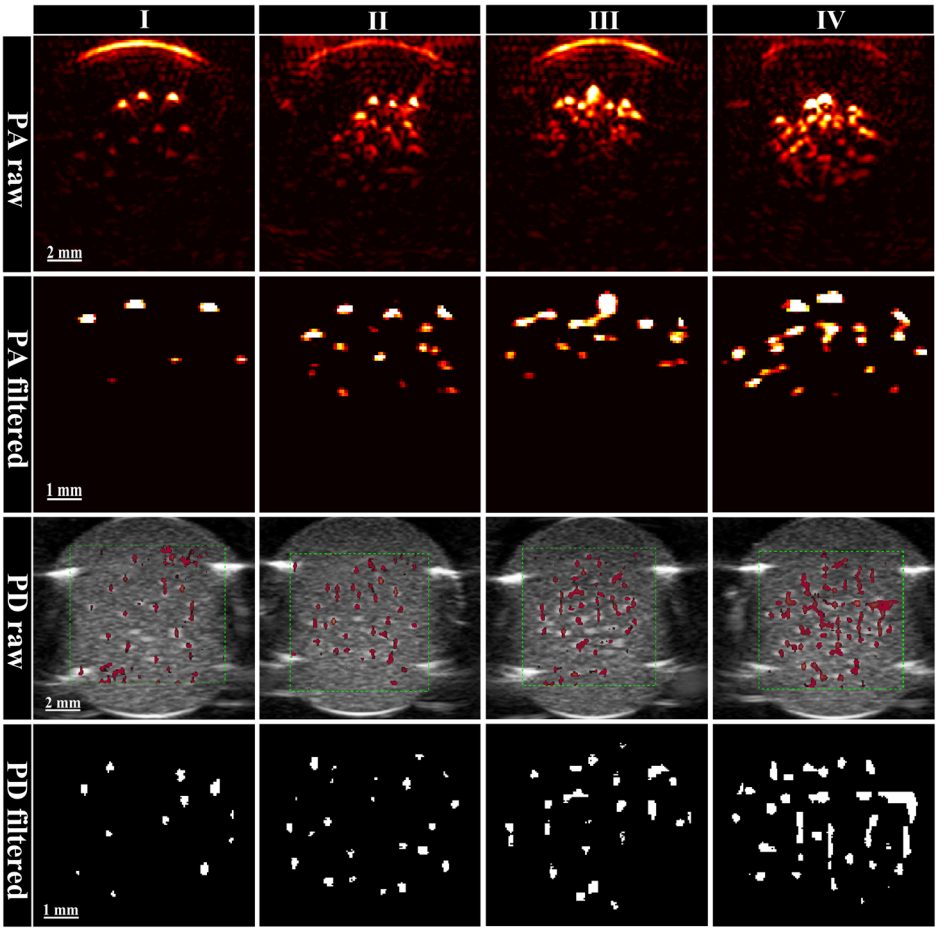

Fig. 6 Cross-sectional PA and PDUS images of the phantoms with increasing perfused area (I to IV). For each modality, the raw total images and the filtered signal in the perfused area are shown. In the raw PDUS images, the dashed squares indicate the PDUS region of interest.

Custom-made perfusion phantoms allowed for controlled measurements on increasing blood volume with both PA and PDUS. The tunable optical and acoustic properties of the gelatin, in combination with an adjustable amount of microchannels, were used to imitate microvascular blood flow in biological tissue. Flow speeds in the channels were adjustable to realistic values for their diameter, in the order of mm/s. The low-budget materials and relatively small production efforts make these phantoms attractive for perfusion-related measurements with different imaging modalities and methods.

The phantom studies revealed the limited imaging depth that is achieved with PA in its current configuration. Only the upper half of the phantom could be imaged, due to attenuation of the optical energy. With the large imaging depth achieved in PDUS, the total phantom was easily imaged. However, PA is of added value in small vasculature detection where blood flow velocities drop below the sensitivity of PDUS.[29]

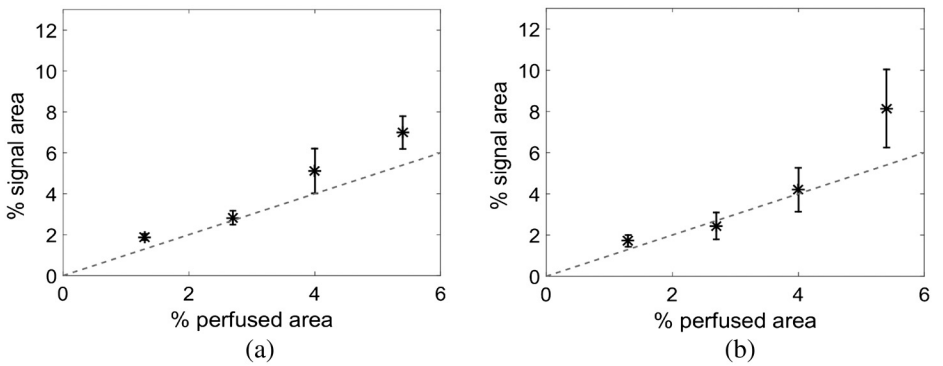

Fig. 7 The relative amount of signal in (a) PA imaging and (b) PD, proportional to the relative amount of perfused cross-sectional area in the phantoms. The signal in PDUS shows an overshoot in the most perfused phantom. Error bars indicate one standard deviation, and the dashed line represents the identity line ($y = x$).

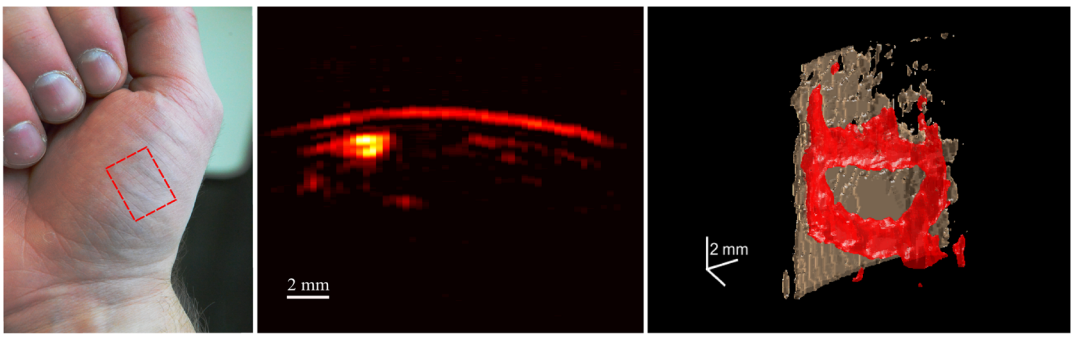

Fig. 8 PA scanning of a small skin area on the hand. (a) Measurement area on the thumb (1.5 × 2.0 cm) and (b) a typical cross-sectional image that is obtained during this scan. The image shows the clear signal from the epidermis and underlying blood vessels. (c) 3-D volumes of the scanned area are obtained by combining and segmenting all cross-sectional 2-D images.

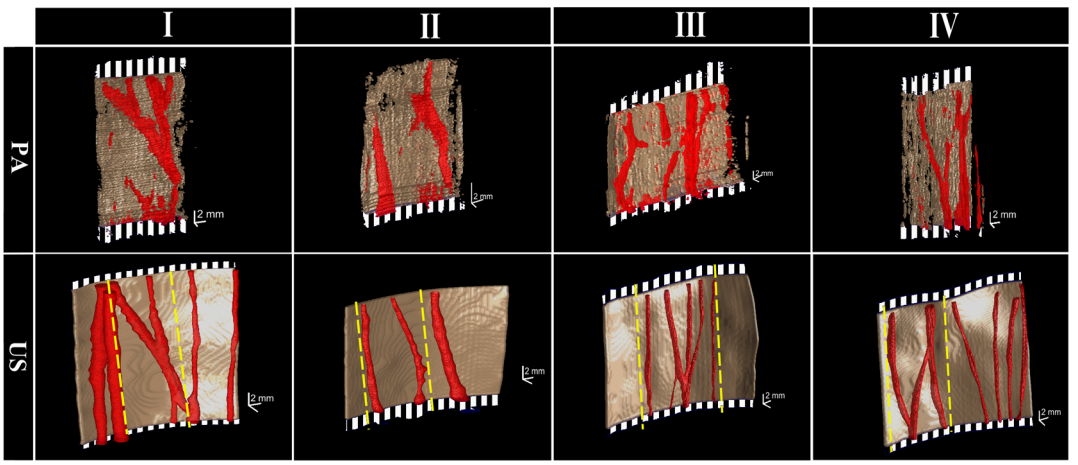

Fig. 9 3-D visualization of PA and US acquisition of subdermal vasculature in the wrist of four volunteers. Point of view is inside the arm. Skin markers are represented white striped while the dotted lines in the US images indicate the corresponding area in the PA scan

With the *in vivo* measurements, the ability to visualize melanin layers and small vasculature with the hand-held probe was demonstrated. Areas of the skin and underlying vasculature were scanned and visualized in 3-D to a depth of about 5 mm. The visualized geometry in the PA images was validated with segmented geometries from US imaging, which showed good agreement. The resolution in the US images was better, which is due to the higher center frequency and smaller pitch of the US probe. Also the manual segmentation in US versus the intensity thresholded segmentation in PA leads to different image qualities. The need for labor intensive segmentation in US versus simple intensity thresholding in PA underlines the advantage of the PA imaging specificity to vasculature.

The PA images of the wrist and hand palm show submillimeter vasculature beneath the epidermis. The spatial resolution of the system prevents imaging of the very small vasculature. Visualization of individual capillaries, arterioles, and venules in the superficial and deep dermal vascular plexi would not be possible since the diameters of these vessels do not exceed 50 μm.[30] Accumulated signal of the deep vascular plexus, interconnecting vessels, and vessels in the subcutaneous tissue, however, are detectable.

The obtained spatial resolution is partly defined by the US detector characteristics of the PA probe. US detectors with higher center frequency and bandwidth would offer improved resolution, at the consequence of a limited imaging depth.[31,32] The impressive spatial resolutions that are achieved in PAM often come at the burden of even higher acquisition times and reduced portability. Different PA implementations need to prove their clinical feasibility and will probably have their own optimal clinical application. PA in the FULLPHASE implementation is capable of imaging submillimeter vasculature to a depth of several millimeters, in real time or in 3-D, with scanning times under 10 s per cm^2.

Future work will focus on *in vivo* assessment of vascularization in skin and subdermal tissue to compare healthy and diseased skin. Furthermore, a multiwavelength PA approach will allow for extending the visual information with assessment of oxygen saturation in the visualized blood vessels.

Disclosures

No conflicts of interest, financial or otherwise, are declared by the authors.

Acknowledgments

This study was funded by the European Community's Seventh Framework Programme (FP7/2007-2013) under Grant Agreement No. 318067.

References

1. L. V. Wang and S. Hu, "Photoacoustic tomography: in vivo imaging from organelles to organs," *Science* **335**(6075), 1458–1462 (2012).
2. P. Beard, "Biomedical photoacoustic imaging," *Interface Focus* **1**(4), 602–631 (2011).
3. A. Taruttis and V. Ntziachristos, "Advances in real-time multispectral optoacoustic imaging and its applications," *Nat. Photonics* **9**(April), 219–227 (2015).
4. L. V. Wang and L. Gao, "Photoacoustic microscopy and computed tomography: from bench to bedside," *Annu. Rev. Biomed. Eng.* **16**(1), 155–185 (2014).
5. J. Allen and K. Howell, "Microvascular imaging: techniques and opportunities for clinical physiological measurements," *Physiol. Meas.* **35**(7), R91–R141 (2014).
6. A. Dawn et al., "Cutaneous blood flow in dermatomyositis and its association with disease severity," *Skin Res. Technol.* **13**(3), 285–292 (2007).
7. M. Matucci-Cerinic, B. Kahaleh, and F. M. Wigley, "Review: evidence that systemic sclerosis is a vascular disease," *Arthritis Rheum.* **65**(8), 1953–1962 (2013).
8. B. Zabihian et al., "In vivo dual-modality photoacoustic and optical coherence tomography imaging of human dermatological pathologies," *Biomed. Opt. Express* **6**(9), 3163 (2015).
9. K. Maslov, G. Stoica, and L. V. Wang, "*In vivo* dark-field reflection-mode photoacoustic microscopy," *Opt. Lett.* **30**(6), 625–627 (2005).
10. H. F. Zhang et al., "Functional photoacoustic microscopy for high-resolution and noninvasive in vivo imaging," *Nat. Biotechnol.* **24**(7), 848–851 (2006).
11. C. P. Favazza, L. A. Cornelius, and L. V. Wang, "In vivo functional photoacoustic microscopy of cutaneous microvasculature in human skin," *J. Biomed. Opt.* **16**(2), 026004 (2011).
12. K. Maslov et al., "Optical-resolution photoacoustic microscopy for in vivo imaging of single capillaries," *Opt. Lett.* **33**(9), 929–931 (2008).
13. C. Li and L. V. Wang, "Photoacoustic tomography and sensing in biomedicine," *Phys. Med. Biol.* **54**(19), R59–R97 (2009).
14. E. Zhang, J. Laufer, and P. Beard, "Backward-mode multiwavelength photoacoustic scanner using a planar Fabry–Perot polymer film ultrasound sensor for high-resolution three-dimensional imaging of biological tissues," *Appl. Opt.* **47**(4), 561 (2008).
15. E. Z. Zhang et al., "In vivo high-resolution 3D photoacoustic imaging of superficial vascular anatomy," *Phys. Med. Biol.* **54**(4), 1035–1046 (2009).
16. X. L. Deán-Ben and D. Razansky, "Functional optoacoustic human angiography with handheld video rate three dimensional scanner," *Photoacoustics* **1**(3–4), 68–73 (2013).
17. A. Buehler et al., "Real-time handheld multispectral optoacoustic imaging," *Opt. Lett.* **38**(9), 1404 (2013).
18. J. J. Niederhauser et al., "Combined ultrasound and optoacoustic system for real-time high-contrast vascular imaging *in vivo*," *IEEE Trans. Med. Imaging* **24**(4), 436–440 (2005).
19. M. K. A. Singh, W. Steenbergen, and S. Manohar, "Handheld probe-based dual mode ultrasound/photoacoustics for biomedical imaging," in *Frontiers in Biophotonics for Translational Medicine*, M. Olivo and U. S. Dinish, Eds., pp. 209–247, Springer, Singapore (2016).
20. K. Daoudi et al., "Handheld probe integrating laser diode and ultrasound transducer array for ultrasound/photoacoustic dual modality imaging," *Opt. Express* **22**(21), 26365 (2014).
21. J. M. Rubin et al., "Fractional moving blood volume: estimation with power Doppler US," *Radiology* **197**(1), 183–190 (1995).
22. C. Martinoli et al., "Power Doppler sonography: clinical applications," *Eur. J. Radiol* **27**(Suppl. 2), S133–S140 (1998).
23. J. R. Cook, R. R. Bouchard, and S. Y. Emelianov, "Tissue-mimicking phantoms for photoacoustic and ultrasonic imaging," *Biomed. Opt. Express* **2**(11), 3193–3206 (2011).
24. A. N. Bashkatov, E. A. Genina, and V. V. Tuchin, "Optical properties of skin, subcutaneous, and muscle tissues: a review," *J. Innovative Opt. Health Sci.* **4**(1), 9–38 (2011).
25. B. J. McGuire and T. W. Secomb, "Estimation of capillary density in human skeletal muscle based on maximal oxygen consumption rates," *Am. J. Physiol. Heart Circ. Physiol.* **285**(6), H2382–H2391 (2003).
26. P. Brodal, F. Ingjer, and L. Hermansen, "Capillary supply of skeletal muscle fibers in untrained and endurance-trained men," *Am. J. Physiol.* **232**(6), H705–H712 (1977).
27. A. Roggan et al., "Optical properties of circulating human blood in the wavelength range 400–2500 nm," *J. Biomed. Opt.* **4**(1), 36–46 (1999).
28. M. P. Fronheiser et al., "Real-time optoacoustic monitoring and three-dimensional mapping of a human arm vasculature," *J. Biomed. Opt.* **15**(2), 021305 (2010).
29. Y. Jiang et al., "Photoacoustic and high-frequency power Doppler ultrasound biomicroscopy: a comparative study," *J. Biomed. Opt.* **15**(5), 056008 (2010).
30. I. M. Braverman, "The cutaneous microcirculation," *J. Invest. Dermatol. Symp. Proc.* **5**(1), 3–9 (2000).
31. H. Zafar et al., "Linear-array-based photoacoustic imaging of human microcirculation with a range of high frequency transducer probes," *J. Biomed. Opt.* **20**(5), 051021 (2015).
32. L. Song et al., "Ultrasound-array-based real-time photoacoustic microscopy of human pulsatile dynamics in vivo," *J. Biomed. Opt.* **15**(2), 021303 (2010).

H. Maarten Heres received his MSc degree in biomedical engineering from the University of Twente, The Netherlands. He is a PhD candidate at Eindhoven University of Technology. His current research interests include the clinical validation of photoacoustics and ultrasound techniques in the assessment of skeletal muscle and skin perfusion. He is a member of the Dutch Society for Medical Ultrasound (NVMU) and IEEE.

Mustafa Umit Arabul received his BSc degree in electrical and electronics engineering from the Middle East Technical University, Ankara, and his MSc degree in biomedical engineering from the Institute of Biomedical Engineering of Bogazici University, Istanbul. He is a PhD candidate at the Eindhoven University of Technology. His current research interests include *in vivo* photoacoustic imaging of carotid arteries and fundamental characterization and clinical validation of photoacoustic imaging. He is a member of SPIE, NVMU, and IEEE.

Marcel C. M. Rutten received his MSc degree in mechanical engineering from Eindhoven University, Eindhoven, The Netherlands, in 1993. He continued on a PhD project on fluid structure interaction in large arteries, and received his PhD in 1998 from the Department of Mechanical Engineering of Eindhoven University of Technology. Since then, he teaches cardiovascular mechanics in the Department of Biomedical Engineering at Eindhoven University.

Frans N. van de Vosse received his PhD in 1987 with his study on the numerical analysis of carotid artery flow. He is a professor of Cardiovascular Biomechanics Group of Eindhoven University of Technology (TU/e). He studied applied physics at TU/e from 1976 to 1982. His current research interests are related to the computational and experimental biomechanical analysis of the cardiovascular system and its application to clinical diagnosis and intervention, cardiovascular prostheses, extracorporeal systems, and medical devices.

Richard G. P. Lopata received his BSc and MSc degrees in biomedical engineering from TU/e, and his PhD from Radboud University Nijmegen Medical Centre with his work on "3D Functional Imaging of the Heart." He is an assistant professor of the Pulse Lab of Eindhoven University of Technology (TU/e). His current research focuses on the multimodality imaging and medical image analysis (strain imaging, elastography, 2-D and 3-D ultrasound and photoacoustics) in cardiovascular applications.